Short communication

Tin dispersed in an oxide matrix as negative electrode material for Li-ion batteries

M. Mouyane, L. Aldon[*], M. Womes, B. Ducourant, J.-C. Jumas, J. Olivier-Fourcade

ICG-AIME (UMR 5253) Université Montpellier II, CC01502, Place E. Bataillon, 34095 Montpellier Cedex 5, France

ARTICLE INFO

ABSTRACT

This paper deals with new tin-based composite β-Sn/(CaSiO$_3$)$_{0.4}$ negative electrode materials for Li-ion batteries. The nature of the oxide matrix and of dispersed tin particles has been investigated by X-ray diffraction (XRD), scanning electron microscope (SEM) coupled with energy dispersion spectroscopy (EDS) and Mössbauer spectroscopy by both transmission (TMS) and backscattering (CEMS) mode for bulk and interface characterizations. The electrochemical behaviour of the composite has been studied during Li-reaction processes. Electrochemical investigation and Mössbauer data analyses suggest the formation of Li$_7$Sn$_2$ during Li reaction. The reversible mechanism is based on cycling between β-Sn and Li$_7$Sn$_2$. An interface composed of CaSn^{IV}SiO$_5$ and a Sn^{II} species between tin particles dispersed in the CaSiO$_3$ matrix is responsible of the irreversible capacity observed in this composite during the first discharge.

1. Introduction

Tin-based materials have been suggested as promising alternatives to carbon-based negative electrodes in order to improve electrochemical performances of Li-ion batteries at high cycling rates [1,2]. Sn-based negative electrodes operate in an advantageous voltage range of 0.25–0.5 V versus lithium, avoiding short-circuits and burn out. However, the large volume variation that occurs during lithiation and de-lithiation causes a structural instability of the electrode and leads to poor cycling performances. In order to solve this problem, intensive studies are focussed on dispersing the electrochemically active element (Sn) in an inactive matrix which acts as a buffer and absorbs or minimizes the volume variations [3]. Composite materials such as Sn/(BPO$_4$)$_{0.4}$ where the borophosphate matrix plays the role of the volume buffer, turned out to have an improved reversible cycling behaviour as compared to pure β-Sn [4]. Preliminary results have been previously reported in the literature [5].

In the present study, this concept of composite materials is extended towards new materials. It will be shown that Sn-CaSiO$_3$ can be used as negative electrode material in Li-ion batteries. This new composite electrode shows rather good and stable electrochemical performances. Electrodes were investigated at various levels of lithiation and de-lithiation by X-ray diffraction (XRD), [119]Sn Mössbauer spectroscopy (MS), scanning electron microscope (SEM) and energy dispersion spectroscopy (EDS) as experimen-

tal techniques. All these results enable us to propose a detailed discharge–charge mechanism for this new class of materials.

2. Experiments

2.1. Synthesis

The Sn/(CaSiO$_3$)$_x$ composite materials were prepared in two steps. First, the CaSiO$_3$ matrix was synthesised by a sol–gel process, using as precursors Si(OC$_2$H$_5$)$_4$ (TEOS) dissolved in an EtOH/HNO$_3$/H$_2$O bath and Ca(NO$_3$)$_2$, 4H$_2$O dissolved in H$_2$O. The resulting gel was dried at 80 °C for 4 h. The resulting powder was ground in an agate mortar and then sieved on a 50 μm mesh sieve. The product was then mixed with β-Sn (Aldrich, 10 μm powder) in a CaSiO$_3$/Sn molar ratio of $x = 0.4$ and heated in a vitreous carbon boat to 850 °C for 7 h under Ar atmosphere. Compared to various compositions we have studied, this specific composition ($x = 0.4$) presents the best electrochemical performances.

2.2. Characterization

The pristine material was characterized for its structural, textural, chemical, microstructural, and electrochemical properties. Sn/(CaSiO$_3$)$_{0.4}$ and lithiated/de-lithiated samples were characterized by XRD with a Panalytical θ–2θ diffractometer using Cu Kα radiation ($\lambda = 1.5418$ Å) and a nickel filter. Crystallographic reference data for the phase speciation were taken from JCPDS cards (International Centre of Diffraction Data). The morphological studies were carried out by SEM with a FEI Quanta FEG 200 field emission gun (FEG) coupled with EDS. Electrochemical tests were

* Corresponding author. Tel.: +33 467143354.
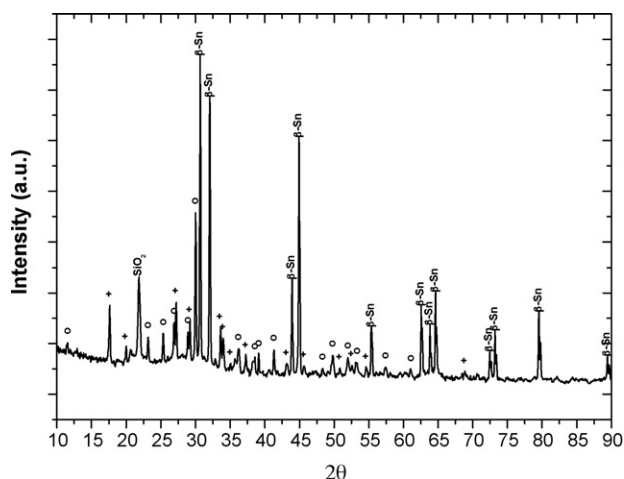*E-mail addresses:* laurent.aldon@univ-montp2.fr, aldon@iut-nimes.fr (L. Aldon).

Fig. 1. XRD pattern of as prepared Sn/(CaSiO$_3$)$_{0.4}$. Open circles and crosses correspond to diffraction peaks of β-CaSiO$_3$ and CaSnSiO$_5$, respectively.

carried out with a solution containing 50 vol% ethylene carbonate (EC), 50 vol% dimethyl carbonate (DMC) and 1 M LiPF$_6$ was used as the electrolyte solution and a Whatman paper (glass microfiber filters) was used as the separator. The Swagelok^{TM} test cell was made of a lithium foil as counter electrode, the working electrode was made by mixing active materials, acetylene black as the conductive agent, and polyvinylidene fluoride (PVDF) as the binder as described in Ref. [6]. The weight ratio of active powder, conductive agent and binder is 80:10:10. Galvanostatic discharge/charge curves were obtained with cycling rates of 1 Li/10 h (C/10) and 1 Li/h (C). Electrochemical charge/discharge cycles were stopped at several characteristic points on the curve. The electrode material was then extracted from the test cell and transferred under argon atmosphere to specific, air-tight sample holders for further analysis by XRD, ^{119}Sn TMS and ^{119}Sn CEMS. ^{119}Sn Mössbauer spectra were recorded in the constant acceleration mode using equipment supplied by Ortec and Wissel. Spectra in transmission geometry were recorded using a NaI(Tl) scintillation detector, spectra in backscattering geometry were recorded using a specific gas counter for the detection of conversion electrons. The γ-ray source consisted of Ba^{119m}SnO$_3$ with a nominal activity of 10 mCi. The velocity scale was calibrated with the magnetic sextet spectrum of a high-purity iron foil absorber recorded with a ^{57}Co(Rh) source. The hyperfine

parameters isomer shift (δ) and quadrupole splitting (ΔE_q) were determined by fitting Lorentzian lines to the experimental data, using the ISOfit programme [7]. The goodness of the fit was controlled by the usual χ^2-test. All isomer shifts are given relative to BaSnO$_3$.

3. Results and discussion

3.1. Pristine material

Fig. 1 shows the XRD pattern of the pristine Sn/(CaSiO$_3$)$_{0.4}$ composite. It reveals the signals which pertain to the β-Sn, β-CaSiO$_3$, CaSnSiO$_5$ and SiO$_2$ phases. Data analyses are consistent with literature data (JCPDS cards 86-2265 β-Sn, 76-0186 β-CaSiO$_3$, 87-0131 CaSnSiO$_5$ and 76-0939 SiO$_2$).

Fig. 2a shows the morphology of the composite as revealed by SEM analysis. The sample has an aggregated structure with evident particle agglomeration. Three different domains can be distinguished, appearing as dark grey, light grey and white areas on the micrograph. Both the white round particles and the light grey domains are embedded in a dark grey matrix. Fig. 2b shows EDS spectra of these three domains, the atomic percentages derived from these spectra are given in Table 1. The white particles consist essentially of tin. Both grey domains are mainly composed of oxygen, silicon, tin and calcium. However, the tin concentration is significantly lower in the dark grey matrix than in the light grey particles. The atomic percentages of the dark grey matrix are close to the theoretical values expected for β-CaSiO$_3$, while the percentages of the light grey particles agree quite well those of CaSnSiO$_5$. Those two compounds were also identified by XRD (Fig. 1). Thus, the composite consists in a mixture of three main phases: a new compound CaSnSiO$_5$, β-CaSiO$_3$ and metallic tin.

In order to get a better insight into the microstructure of the composite we have collected ^{119}Sn Mössbauer spectra by TMS and by CEMS. As can be seen in Fig. 3, these spectra reveal the presence of three tin-containing species. The hyperfine parameters are given in Table 2. The first species is characterized by a singlet with an isomer shift of 2.58 mm s^{-1}, which close to the value of 2.56 mm s^{-1} generally observed for β-Sn [8,9]. The hyperfine parameters of the first doublet, $\delta = -0.06$ mm s^{-1} and $\Delta E_q = 1.44$ mm s^{-1} agree well with data reported in the literature for CaSn^{IV}SiO$_5$ [10], confirming our observations by XRD and EDS. A second doublet observed at high velocity (2.95 mm s^{-1}) is attributed to a Sn^{II} species. Since this species is not observed by XRD we suggest that Sn^{II} is amor-
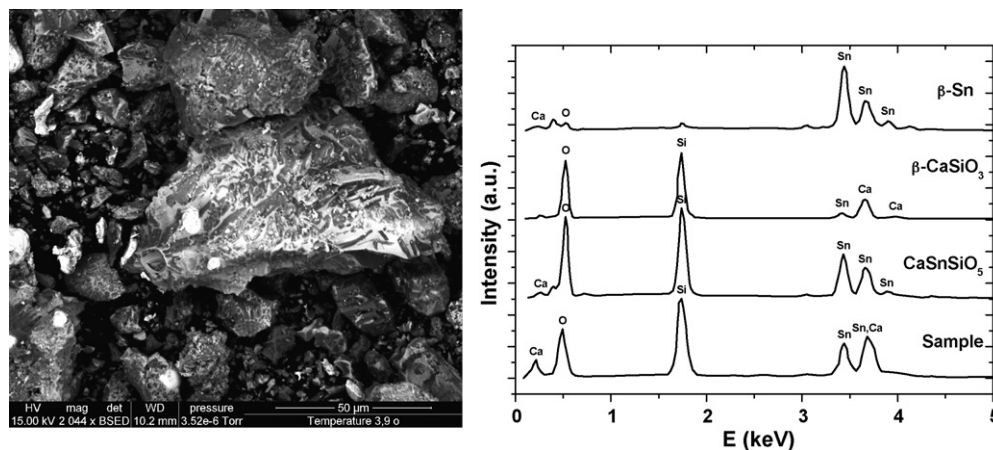

Fig. 2. (a) Scanning electron micrographs of Sn/(CaSiO$_3$)$_{0.4}$ sample obtained in backscattering mode. Both white rounded particles and light grey micro-crystal are embedded in a dark grey matrix correspond respectively to β-Sn, CaSnSiO$_5$ and β-CaSiO$_3$. (b) Energy dispersion spectra from bottom to top of the whole sample (Sn/(CaSiO$_3$)$_{0.4}$), the light grey area (CaSnSiO$_5$), the dark grey area (β-CaSiO$_3$) and the small white spherical particles (β-Sn).

Table 1
Atomic percentages obtained from EDS analyses on whole sample, and areas of interest by moving the analyzing spot

Investigated area	O	Si	Ca	Sn	Attribution
Whole sample	43.8(*40.0*)[a]	13.9(*13.3*)	9.9(*13.3*)	32.5(*33.3*)	$Sn/(CaSiO_3)_{0.4}$
White particle	10.5(*0.0*)	1.3(*0.0*)	0.6(*0.0*)	87.6(*100.0*)	β-Sn
Light grey area	58.8(*67.5*)	15.8(*12.5*)	4.3(*12.5*)	21.1(*12.5*)	$CaSnSiO_5$
Dark grey area	58.5(*60.0*)	20.6(*20.0*)	11.6(*20.0*)	9.3(*0.0*)	β-$CaSiO_3$

[a] Values in italic are those theoretically expected in the case of isolated particles. Variations are in agreement with the presence of interfaces between phases detected by XRD. Ca/Sn ratio is rather difficult to estimate due to overlap between emission lines of Ca($K\alpha$) 3.69 keV and Sn($L\beta_1$) 3.66 keV and also Ca($K\beta$) 4.01 keV and Sn($L\beta_2$) 3.90 keV. Ca percentage seems to be underestimated since Si/Ca should be 1.
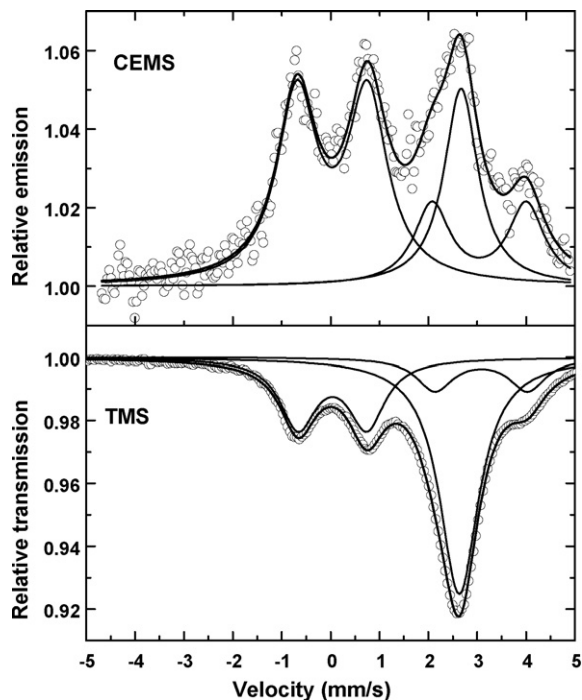
Fig. 3. ^{119}Sn Mössbauer spectra collected in the transmission (TMS: bulk) and in backscattering mode (CEMS: surface).

Fig. 4. Schematic picture of the $Sn(CaSiO_3)_{0.4}$ composite deduced for X-ray diffraction, energy dispersive spectroscopy and ^{119}Sn Mössbauer spectroscopy. White spherical particles (β-Sn) are embedded in $CaSiO_3$ matrix (in black). An interface containing Sn^{II} detected by Mössbauer spectroscopy is located (broad line) between the β-tin and the phase $CaSnSiO_5$ (in grey).

phous. Some analogies can be drawn from a comparison with $Sn/(BPO_4)_{0.4}$ composites [11]. This Sn^{II} species has already been observed in Sn-based amorphous silicates [12,13]. After correction of the absorption by the Lamb–Mössbauer factors f at 300 K ($f(Sn^0) = 0.04$, $f(Sn^{IV}) = 0.70$ and $f(Sn^{II}) = 0.20$), we found that 92% of the tin in the sample belongs to β-Sn, 3% to $CaSn^{IV}SiO_5$ and 5% to the Sn^{II} amorphous silicate species. The surface analysis by CEMS confirms the dispersion of tin particles in the oxide matrix. The β-Sn contribution is lower (81%) in the probed surface than that observed in the bulk (whole sample). On the other hand, the contributions of both Sn^{IV} (8%) and Sn^{II} (11%) are higher at the surface than in the bulk.

Based on all these experimental results we can propose a schematic picture of the pristine $Sn/(CaSiO_3)_{0.4}$ composite shown in Fig. 4. Spherical tin particles seem to be homogeneously distributed over the sample. The new compound $CaSnSiO_5$ and the
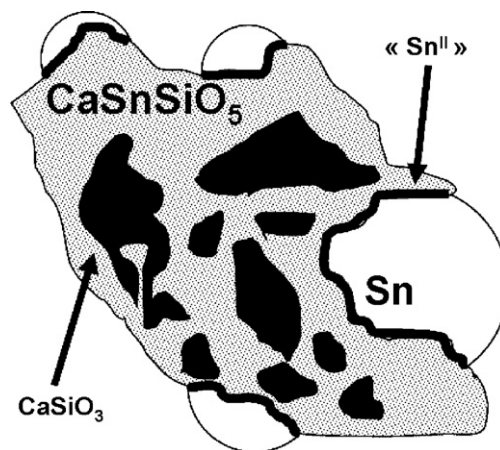
amorphous Sn^{II} species are located at the interface between these spherical particles of β-Sn and the matrix composed of β-$CaSiO_3$.

3.2. Electrochemical behaviour

The electrochemical behaviour of this composite has been tested at C/10 and C rate. For clarity we give in this paper the first discharge/charge cycle and the second discharge only, as shown in Fig. 5. We summarize some results in Table 3. At C rate, we have recorded up to 20 cycles at the end of which a capacity of about 232 mAh g^{-1} was found. For the sample tested at C/10 rate, investigations by ex situ XRD and ^{119}Sn TMS are shown in Fig. 6.

3.2.1. First discharge

XRD reveals that $CaSiO_3$ plays the role of an inactive matrix versus Li reaction since the phase is still present at the end of the discharge (Fig. 6c). The minority phase $CaSn^{IV}SiO_5$ and the Sn^{II} phase located at the interface between tin particles are reduced before the plateau at 0.4 V, contributing in this way to the irreversible capacity of the composite. At the end of the first discharge the Li_7Sn_2 alloy is formed [14] (main diffraction line at $\sim 38.4°2\theta$), while a small amount of β-Sn is not reduced by lithium. After

Table 2
Experimental capacities calculated from whole composite mass (165.18 g mol^{-1}) at the first, second, fourth and eighth discharge obtained at two regimes C/10 (1 Li/10 h) and C (1 Li/h) in potential windows [0.01–1.2 V]

Rate	C_1 (mAh g^{-1})	C_2 (mAh g^{-1})	C_4 (mAh g^{-1})	C_8 (mAh g^{-1})
C/10	611(3.76)[75.8%][a]	467(2.86)[101.5%]	482(2.95)[98.3%]	464(2.84)[95.6%]
C	444(2.72)[53.1%]	361(2.21)[108.3%]	361(2.21)[101.9%]	343(2.10)[98.8%]

[a] Results in round brackets denote the number of inserted lithium ions per $Sn(CaSiO)_{0.4}$ formula unit. Values in square brackets denote the coulombic efficiency determined by the ratio of charge capacity to discharge capacity.
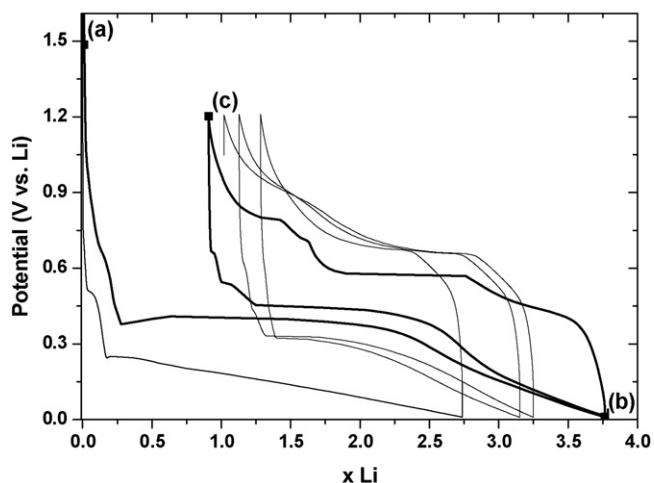
Fig. 5. Discharge/charge curves of Sn(CaSiO$_3$)$_{0.4}$ composite material tested in the range 1.2–0.01 V obtained in galvanostatic mode at a rate of C/10 (thick line) and C (thin line). Pristine material (a), end of first discharge (b) and end of first charge (c) have been characterized ex situ by both XRD and ^{119}Sn Mössbauer spectroscopy.

Table 3
Hyperfine parameters obtained from ^{119}Sn Mössbauer spectra shown in Fig. 3

Mössbauer mode	Tin sites	Sn(CaSiO$_3$)$_{0.4}$			
		δ (mm s^{-1})	Δ (mm s^{-1})	A%	RC%
TMS	Sn^0	2.58(3)	–	56	92
	Sn^{II}	2.95(3)	1.93(3)	14	5
	Sn^{IV}	−0.06(2)	1.44(3)	30	3
CEMS	Sn^0	2.54(4)	–	29	81
	Sn^{II}	2.99(4)	1.90(2)	19	11
	Sn^{IV}	−0.05(3)	1.40(4)	52	8

The different types of tin used in the Mössbauer fitting procedure and their relative contributions in the total absorption (A%) in the Mössbauer spectra, the values of the isomer shift δ, the quadrupole splitting Δ and the relative concentration (RC) calculated using the following values of the Lamb–Mössbauer factor f: f(Sn^0) = 0.04, f(Sn^{II}) = 0.2 and f(Sn^{IV}) = 0.7. Isomer shifts are given relative to the reference BaSnO$_3$.

reaction of 3.8 Li with the composite material (point b of Fig. 5), the mean isomer shift observed for the main component at about 1.9 mm s^{-1} in the Mössbauer spectrum confirms the formation of Li$_7$Sn$_2$ alloy at the end of the discharge (Fig. 6b, Table 4) [8]. The absorption was corrected by the Lamb–Mössbauer factors at 300 K (f(β-Sn) = 0.04 [11,15] and f(Li$_7$Sn$_2$ = 0.12) [16]). We found that

12($\pm$2)% of tin belongs to β-Sn and 88($\pm$2)% to Li$_7$Sn$_2$. The first discharge corresponds to a certain reorganization of the starting material. We suppose that a very small amount of Li has reacted in the vicinity of CaSiO$_3$ matrix improving its conductivity. This phenomenon was already observed in Sn/(BPO$_4$)$_{0.4}$ composite [17].

3.2.2. Charge

During the first charge, after extraction of Δx = 3.02 Li, corresponding to a coulombic efficiency of 75.8% for the first cycle, the ^{119}Sn Mössbauer spectrum (Fig. 6c) shows only the presence of β-Sn (100%) in agreement with the XRD pattern. This is in a rather good agreement with the theoretical number of lithium
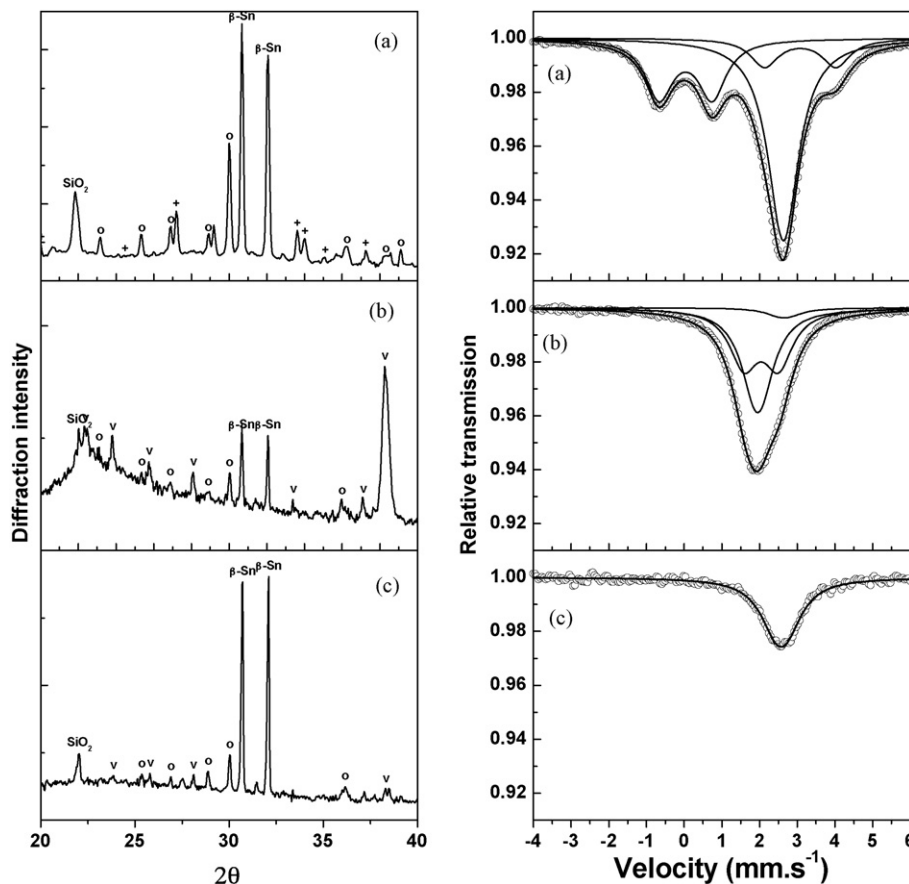

Fig. 6. XRD patterns and ^{119}Sn Mössbauer spectra of the pristine composite (a), end of first discharge (b) and end of first charge (c). Open circles and crosses correspond to diffraction peaks of β-CaSiO$_3$ and CaSnSiO$_5$, respectively. The symbol "v" was used for Li$_7$Sn$_2$ alloy. ^{119}Sn Mössbauer spectrum (b) shows 2 contributions: 20% β-Sn (δ = 2.56 mm s^{-1}) and 80% Li$_7$Sn$_2$ (δ_1 = 1.84 mm s^{-1}, Δ_1 = 0.28 mm s^{-1}; δ_2 = 1.96 mm s^{-1}, Δ_2 = 1.13 mm s^{-1}). These experimental values are close to those published in Ref. [8].

Table 4
Hyperfine parameters obtained from ^{119}Sn Mössbauer spectra shown in Fig. 3

Li reaction	Tin sites	Sn(CaSiO$_3$)$_{0.4}$			
		δ (mm s^{-1})	Δ (mm s^{-1})	A%	RC%
End of first discharge	Sn^0	2.56(1)	0.23(2)	5	12
	Li$_7$Sn$_2$ (Sn$_1$)	1.86(1)	0.19(2)	47.5	44
	Li$_7$Sn$_2$ (Sn$_2$)	1.95(1)	0.91(2)	47.5	44
First charge	Sn^0	2.48(1)	0.29(2)	100	100

The different types of tin used in the Mössbauer fitting procedure and their relative contributions in the total absorption (A%) in the Mössbauer spectra, the values of the isomer shift δ, the quadrupole splitting Δ and the relative concentration (RC) calculated using the following values of the Lamb–Mössbauer factor f: $f(\text{Sn}^0) = 0.04$ and $f(\text{Li}_7\text{Sn}_2) = 0.12$. Isomer shifts are given relative to the reference BaSnO$_3$.
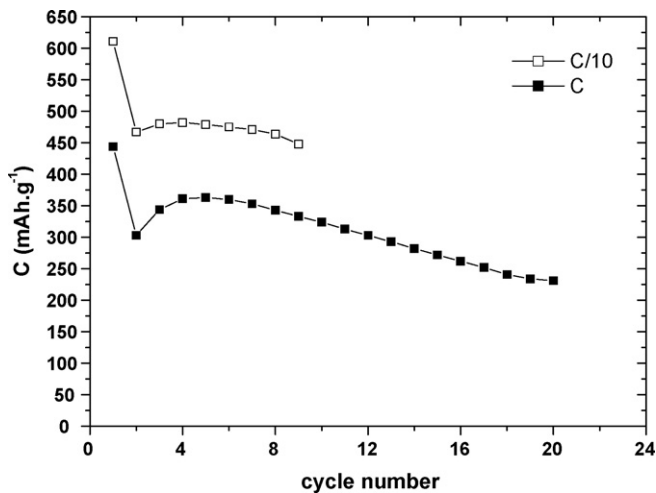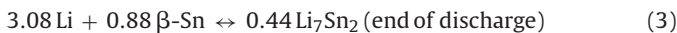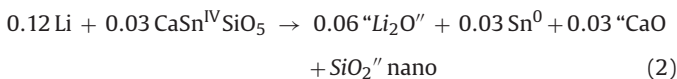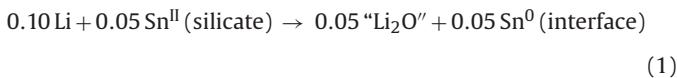

Fig. 7. Cycle life of the composite Sn/(CaSiO$_3$)$_{0.4}$ at C/10 (open square) and C rate (solid square).

atoms $\Delta x = 0.88 \times 3.5 = 3.08$ Li which is to be extracted for the back-transformation of 88% of Li$_7$Sn$_2$ to β-Sn.

3.2.3. Proposed mechanism

We suggest the following electrochemical reaction mechanism for Li in the composite:

$$0.10\,\text{Li} + 0.05\,\text{Sn}^{II}\,(\text{silicate}) \rightarrow 0.05\,\text{``Li}_2\text{O''} + 0.05\,\text{Sn}^0\,(\text{interface}) \tag{1}$$

$$0.12\,\text{Li} + 0.03\,\text{CaSn}^{IV}\text{SiO}_5 \rightarrow 0.06\,\text{``Li}_2\text{O''} + 0.03\,\text{Sn}^0 + 0.03\,\text{``CaO}$$
$$+ \text{SiO}_2\text{''}\,\text{nano} \tag{2}$$

$$3.08\,\text{Li} + 0.88\,\beta\text{-Sn} \leftrightarrow 0.44\,\text{Li}_7\text{Sn}_2\,(\text{end of discharge}) \tag{3}$$

The amount of unreacted β-Sn during lithium reaction is $0.05 + 0.03 + (0.92 - 0.88) = 0.12$ in agreement with Mössbauer data. In this case, we assume that during the first discharge $3.8 - (0.1 + 0.12 + 3.08) = 0.5$ Li have reacted with carbon black used for cell preparation at a potential of above 0.7 V (SEI film) [18], between 0.7 and 0.45 V for Sn^{II}/Sn^{IV} reduction and have contributed to the decomposition of the electrolyte at lower potential [19]. In

Fig. 7, we have represented the cycle life of the composite under study. Depending on the electrochemical regime, capacity retention shows rather interesting performances. Hence, at C/10, we recover about 96% of the capacity at the 8th cycle. At C rate, we observe first an increase of the capacity upon cycling, then a decrease with about 77.2% of the capacity at the 18th cycle.

4. Conclusion

This work deals with a forefront subject in battery materials, as it provides interesting information on β-Sn/(CaSiO$_3$)$_{0.4}$ composite electrodes for Li ion batteries. XRD, scanning electron microscopy coupled to energy dispersion spectroscopy gave us a good description of the composite. β-Sn particles are well dispersed in a CaSiO$_3$ matrix as expected, but an interface composed of Sn^{II} between β-CaSiO$_3$ and β-Sn has been found. The electrochemical reaction of Li into the composite follows several steps: (i) Sn^{II} is reduced during the very first stage of Li reaction, (ii) CaSn^{IV}SiO$_5$ is also reduced and (iii) β-Sn particles partially react with Li by forming a Li$_7$Sn$_2$ alloy well characterized by both XRD and ^{119}Sn Mössbauer spectroscopy. The electrochemical process is then based on the reversible conversion of β-Sn to Li$_7$Sn$_2$. X-ray diffraction and ^{119}Sn Mössbauer spectroscopy gave us valuable information about both long-range order and the local environment of tin in the studied composite.

References

[1] D. Larcher, S. Beattie, M. Morcrette, K. Edström, J.-C. Jumas, J.-M. Tarascon, J. Mater. Chem. 17 (2007) 3759.
[2] R.A. Dunlap, D.A. Smail, D.D. Macneil, M.N. Obrovac, J.R. Dahn, J. Alloys Compd. 289 (1999) 135.
[3] A. Aboulaich, F. Robert, P.-E. Lippens, L. Aldon, J. Olivier-Fourcade, P. Willman, J.-C. Jumas, Hyperfine Interact. 167 (2006) 733.
[4] J.-C. Jumas, F. Robert, P.-E. Lippens, J. Olivier-Fourcade, P. Willman, Patent no. FR2873855.
[5] A. Aboulaich, M. Mouyane, F. Robert, P.-E. Lippens, J. Olivier-Fourcade, P. Willman, J.-C. Jumas, J. Power Sources 174 (2007) 1224.
[6] S. Denis, E. Baudrin, M. Touboul, J.M. Tarascon, J. Electrochem. Soc. 144 (1997) 4099.
[7] W. Kündig, Nucl. Instrum. Methods 75 (1969) 336.
[8] F. Robert, P.E. Lippens, J. Olivier-Fourcade, J.-C. Jumas, F. Gillot, M. Morcrette, J.-M. Tarascon, J. Solid State Chem. 180 (2007) 339.
[9] F. Robert, P.E. Lippens, J. Olivier-Fourcade, J.-C. Jumas, M. Morcrette, J. Power Sources 146 (2005) 492.
[10] D. Niemeier, H. Mehner, U. Bismayer, K.D. Becker, Phys. Status Solidi 211 (b) (1999) 581.
[11] F. Robert, F. Morato, J. Chouvin, L. Aldon, P.E. Lippens, J. Olivier-Fourcade, J.-C. Jumas, B. Simon, Ph. Biensan, J. Power Sources 119–121 (2003) 581.
[12] S. Spiga, R. Mantovan, M. Fanciulli, N. Ferretti, F. Boscherini, F. d'Acapito, B. Schmidt, R. Grotzschel, A. Mucklich, Phys. Rev. B 68 (2003) 205419.
[13] K.F.E. Williams, C.E. Johnson, J.A. Johnson, D. Holland, M.M. Karim, J. Phys.: Condens. Matter 7 (1995) 9485.
[14] F. Robert, P.E. Lippens, R. Fourcade, J.-C. Jumas, F. Gillot, M. Morcrette, J.-M. Tarascon, Hyperfine Interact. 167 (2006) 797.
[15] J. Chouvin, J. Olivier-Fourcade, J.-C. Jumas, B. Simon, O. Godiveau, Chem. Phys. Lett. 308 (1999) 413.
[16] C.M. Ionica-Bousquet, P.E. Lippens, L. Aldon, J. Olivier-Fourcade, J.-C. Jumas, Chem. Mater. 18 (2006) 6442.
[17] E.M. Kelder, M.J.G. Jak, F. De Lange, J. Schoonman, J. Solid State Ionics 85 (1996) 285.
[18] Y.N. Li, J. Yang, J. Zhang, J. Phys. Chem. Solids 67 (2006) 882.
[19] D. Aurbach, I. Weissman, A. Zaban, O. Chusid, Electrochim. Acta 39 (1994) 51.